

# Diverse Spreading Behavior of Binary Polymer Nanodroplets

David R. Heine, Gary S. Grest, Edmund B. Webb III

11th October 2018

Sandia National Laboratories, Albuquerque, New Mexico 87185

## Abstract

Molecular dynamics simulations are used to study the spreading of binary polymer nanodroplets in a cylindrical geometry. The polymers, described by the bead-spring model, spread on a flat surface with a surface-coupled Langevin thermostat to mimic the effects of a corrugated surface. Each droplet consists of chains of length 10 or 100 monomers with  $\sim 350\,000$  monomers total. The qualitative features of the spreading dynamics are presented for differences in chain length, surface interaction strength, and composition. When the components of the droplet differ only in surface interaction strength, the more strongly wetting component forms a monolayer film on the surface even when both materials are above or below the wetting transition. In the case where the only difference is the polymer chain length, the monolayer film beneath the droplet is composed of an equal amount of short chain and long chain monomers even when one component (the shorter chain length) is above the wetting transition and the other is not. The fraction of short and long chains in the precursor foot depends on whether or not both the short and long chains are in the wetting regime. Diluting the concentration of the strongly wetting component in a mixture with a weakly wetting component decreases the rate of diffusion of the wetting material to the surface and limits the spreading rate of the precursor foot, but the bulk spreading rate is not affected until the more strongly wetting component is removed completely.

## 1 Introduction

The spreading of liquid droplets on a surface is an important issue for several industries including adhesion, lubrication, coatings, and printing. Emerging nanotechnology in areas such as lithography and microfluidics make the issue of droplet spreading on small length scales even more relevant.

Just as blending bulk polymers can improve the physical properties of the resulting material, adding a second component to a spreading droplet can produce a desired change in surface tension or wettability. For

example, adding a surfactant to a droplet that ordinarily does not wet a surface can give a product that does wet the surface.<sup>1</sup> In general, adding a second component provides more parameters with which to tune the material properties, but it also introduces more complex phenomena such as the interdiffusion of the two components and possible preferential wetting of one at either the liquid/solid or liquid/vapor interface due to the difference in surface tension.

Compared to homogeneous systems, the published literature on binary droplets is limited. Experiments on binary droplets have been concerned primarily with a nonwetting polymer solute in a wetting solvent. These experiments explored the concentration dependence of the equilibrium contact angle<sup>2</sup> and found a leak-out transition<sup>3,4</sup> where a film of pure solvent is in equilibrium with the droplet. Other experimental<sup>5</sup> and theoretical papers<sup>6,7</sup> focus on the equilibrium behavior of binary mixtures. The surface segregation of two-component polymer films has been studied using molecular dynamics (MD) simulation<sup>8–10</sup> as well as numerical techniques based on Ising-like models.<sup>11–13</sup> Some MD simulations of droplet spreading have been performed for mixtures of solvent and oligomers<sup>14,15</sup> with 4 000 monomers or mixtures of two oligomers<sup>16</sup> with up to 25 000 monomers, though even larger system sizes are required to adequately model the spreading dynamics. One work by the current authors explored reactive wetting of binary droplets in metallic systems.<sup>17</sup> Results therein demonstrated a difference in substrate dissolution rate with varying droplet composition, which in turn resulted in different wetting kinetics and equilibria. However, the combined phenomena of substrate dissolution with wetting prevents directly connecting those results to non-reactive wetting of binary polymer droplets.

This paper presents molecular dynamics simulations of binary polymer nanodroplets differing in either polymer chain length or surface interaction strength. We explore the qualitative differences in the spreading behavior, surface monomer composition, and precursor foot composition for several systems. We also vary the relative concentration of the two components and analyze the velocity distributions of the spreading droplets. All of the simulations presented here are for droplets of  $\sim 350\,000$  monomers, which for single component droplets is sufficiently large to overcome finite size effects.<sup>18,19</sup>

This paper is organized as follows. Section 2 presents a brief summary of the molecular dynamics simulation techniques and the application of the surface-coupled Langevin thermostat. It also describes the methods used to analyze the simulation results. The methods of analysis are described in more detail elsewhere.<sup>18,19</sup> Section 3 contains the simulation results for binary polymer nanodroplets for different polymer chain lengths and surface interaction strengths, and discusses the effects of varying the mole fraction of strongly wetting and weakly wetting components. Conclusions drawn from these simulations are presented in Sec. 4.

## 2 Simulation Details

Molecular dynamics simulations are performed using the standard coarse-grained model for polymer chains in which the polymer is represented by spherical beads of mass  $m$  attached by springs. We use a truncated Lennard-Jones (LJ) potential to describe the interaction between the monomers. The LJ potential is given by

$$U_{LJ}(R) = \begin{cases} 4\epsilon \left[ \left(\frac{\sigma}{r}\right)^{12} - \left(\frac{\sigma}{r}\right)^6 \right] & r \leq r_c \\ 0 & r > r_c \end{cases} \quad (1)$$

where  $\epsilon$  and  $\sigma$  are the LJ units of energy and length and the cutoff is set to  $r_c = 2.5\sigma$ . The monomer-monomer interaction  $\epsilon$  is used as the reference and all monomers have the same diameter  $\sigma$ . For bonded monomers, we apply an additional potential where each bond is described by the finite extensible nonlinear elastic (FENE) potential<sup>20</sup> with  $k = 30\epsilon$  and  $R_0 = 1.5\sigma$ .

The substrate is modeled as a flat surface since it was found previously<sup>18</sup> that with the proper choice of thermostat, the simulations using a flat surface exhibit the same behavior as those using a realistic atomic substrate. Since simulating a realistic substrate requires several times the total number of atoms in the simulation, using the flat surface greatly improves the computational efficiency. The interactions between the surface and the monomers in the droplet at a distance  $z$  from the surface are modeled using an integrated LJ potential,

$$U_{LJ}^{wall}(z) = \begin{cases} \frac{2\pi\epsilon_w}{3} \left[ \frac{2}{15} \left(\frac{\sigma}{z}\right)^9 - \left(\frac{\sigma}{z}\right)^3 \right] & z \leq z_c \\ 0 & z > z_c \end{cases} \quad (2)$$

where  $\epsilon_w$  is the monomer-surface interaction strength and  $z_c = 2.2\sigma$ .

We apply the Langevin thermostat to provide a realistic representation of the transfer of energy in the droplet. The Langevin thermostat simulates a heat bath by adding Gaussian white noise and friction terms to the equation of motion,

$$m_i \ddot{\mathbf{r}}_i = -\Delta U_i - m_i \gamma_L \dot{\mathbf{r}}_i + \mathbf{W}_i(t), \quad (3)$$

where  $m_i$  is the mass of monomer  $i$ ,  $\gamma_L$  is the friction parameter for the Langevin thermostat,  $-\Delta U_i$  is the force acting on monomer  $i$  due to the potentials defined above, and  $\mathbf{W}_i(t)$  is a Gaussian white noise term.<sup>21</sup> Coupling all of the monomers to the Langevin thermostat has the unphysical effect of screening the hydrodynamic interactions in the droplet and not damping the monomers near the surface stronger than

those in the bulk. To overcome this, we use a Langevin coupling term with a damping rate that decreases exponentially away from the substrate.<sup>22</sup> We choose the form  $\gamma_L(z) = \gamma_L^s \exp(\sigma - z)$  where  $\gamma_L^s$  is the surface Langevin coupling and  $z$  is the distance from the substrate. We generally use values of  $\gamma_L^s = 10.0 \tau^{-1}$  and  $3.0 \tau^{-1}$  for  $\varepsilon_w = 2.0 \varepsilon$  and  $3.0 \varepsilon$ , respectively, based on earlier work<sup>18</sup> matching the diffusion constant of the precursor foot for flat and atomistic substrates. The larger  $\gamma_L^s$  corresponds to an atomistic substrate with larger corrugation and hence larger dissipation and slower diffusion near the substrate.

All of the droplets presented here are modeled as hemicylinders as described previously.<sup>19</sup> The droplets spread in the  $x$  direction and each system is periodic in the  $y$  direction with length  $L_y = 40 \sigma$  and open in the other two directions. This allows a larger droplet radius to be studied in the cylindrical geometry than in the spherical geometry using the same number of monomers. The binary droplets consist of either mixtures of chain length  $N = 10$  and  $N = 100$  polymers with the same surface interaction strength  $\varepsilon_w$  or mixtures of chain length  $N = 10$  with varying  $\varepsilon_w$ . Unless explicitly stated, the binary droplets contain an equal number of monomers of each component with initial droplet radius of  $R_0 = 80 \sigma$  for a total size of  $\sim 350\,000$  monomers. These droplets are large enough that finite droplet size effects are minimal.<sup>18</sup>

The equations of motion are integrated using a velocity-Verlet algorithm. We use a time step of  $\Delta t = 0.01 \tau$  where  $\tau = \sigma \left(\frac{m}{\varepsilon}\right)^{1/2}$ . The simulations are performed at a temperature  $T = \varepsilon/k_B$  using the LAMMPS code.<sup>23</sup> Most of the simulations were run on 48 to 64 processors of Sandia's ICC Intel Xeon cluster. One million steps for a wetting drop of 350 000 monomers takes 37 hours on 48 processors.

For the simulations presented here, the instantaneous contact radii for the precursor foot and bulk regions are extracted every  $400 \tau$ . The contact radius is calculated by defining a one-dimensional radial distribution function, as described previously.<sup>18</sup> The precursor foot radius calculation includes all monomers that are within  $1.5 \sigma$  of the surface whereas the bulk radius calculation uses monomers between  $4.5$  and  $6.0 \sigma$  from the surface.

### 3 Results and Discussion

The additional degrees of freedom for binary droplets leads to a number of qualitatively distinct spreading characteristics. In the following figures, we show snapshots of several different droplets as they wet the substrate. In each case, the droplets start in roughly the same configuration with a contact angle near  $90^\circ$ , but they each show differences in the precursor foot composition and spreading rate as well as the composition of the first layer above the substrate.

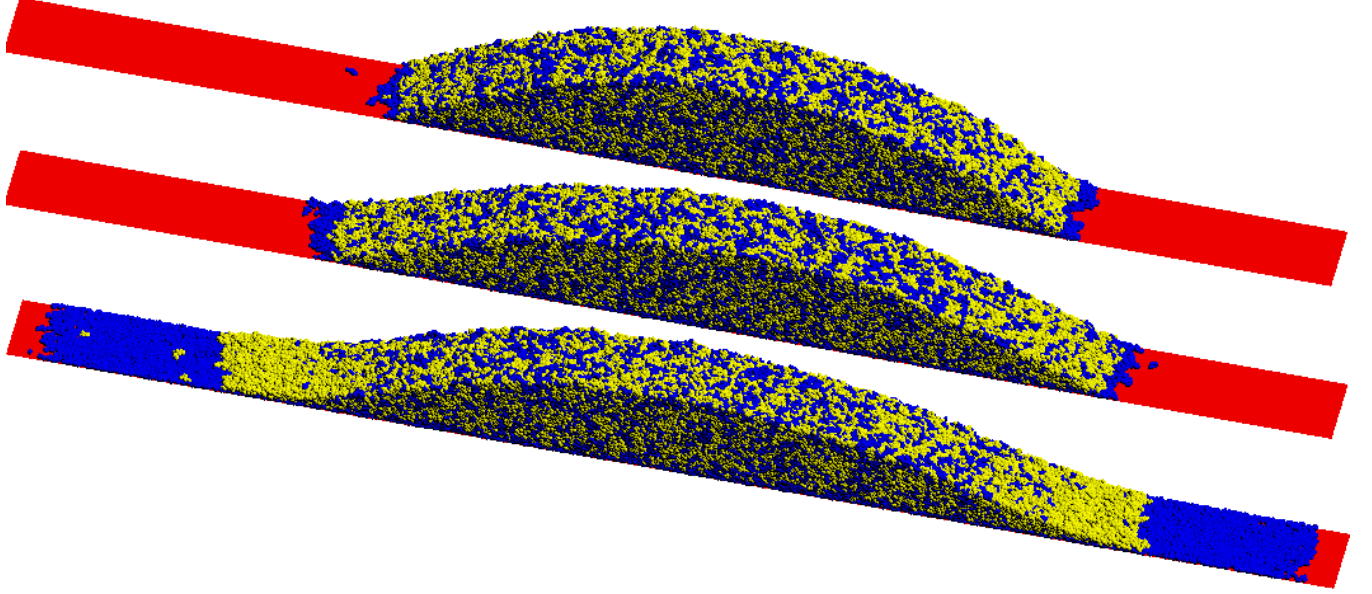


Figure 1: Profiles for binary droplets composed of equal mixtures of chain length  $N = 10$  with  $\varepsilon_w = 1.0 \varepsilon$  (yellow) and  $\varepsilon_w = 2.0 \varepsilon$  (blue) at  $t = 40\,000 \tau$  (top) and  $t = 80\,000 \tau$  (middle). Profile for  $\varepsilon_w = 2.0 \varepsilon$  (yellow) and  $\varepsilon_w = 3.0 \varepsilon$  (blue) at  $t = 40\,000 \tau$  (bottom). The substrate (red) has a length of  $600 \sigma$  and a width of  $40 \sigma$  in each profile.  $\gamma_L^s = 10.0 \tau^{-1}$ .

### 3.1 Substrate Interaction Strength

The top two droplets in Fig. 1 show a profile of a spreading droplet for the mixture of chain length  $N = 10$  in which half of the chains interact with the substrate with  $\varepsilon_w = 1.0 \varepsilon$  and half with  $\varepsilon_w = 2.0 \varepsilon$  for two different times. Previously we have shown that the wetting transition for droplets of chain length  $N = 10$  occurs at  $\varepsilon_w^c \simeq 1.75 \varepsilon$ . This droplet is a mixture of a wetting and nonwetting polymer.<sup>18</sup> For  $N = 10$ ,  $\varepsilon_w = 1.0 \varepsilon$  has a finite contact angle of  $\theta_0 \cong 90^\circ$ . At early times, a monolayer of the wetting component forms at the solid interface and wets the substrate. However, unlike the case of a homogeneous droplet in which all monomers interact with the substrate with  $\varepsilon_w = 2.0 \varepsilon$ ,<sup>19</sup> the precursor foot in this case does not separate from the main droplet. Both components of the droplet follow the monolayer as it wets the substrate, but the spreading rate of the droplet is limited by the spreading rate of the monolayer. The evolution of the contact angle for the binary droplet with  $\varepsilon_w = 1.0 \varepsilon$  and  $\varepsilon_w = 2.0 \varepsilon$  is compared to the single component droplet with  $\varepsilon_w = 2.0 \varepsilon$  in Fig. 2. In this case, adding the lower  $\varepsilon_w$  component slightly decreases the spreading rate of the droplet. This decrease is sufficient to produce a better fit to the hydrodynamic spreading model<sup>19</sup> as compared to the pure  $\varepsilon_w = 2.0 \varepsilon$  system.

Different behavior is observed when both components wet the surface as shown in the bottom panel of Fig. 1 for a mixture with  $\varepsilon_w = 2.0 \varepsilon$  and  $3.0 \varepsilon$ . Despite the fact that both components wet the substrate,

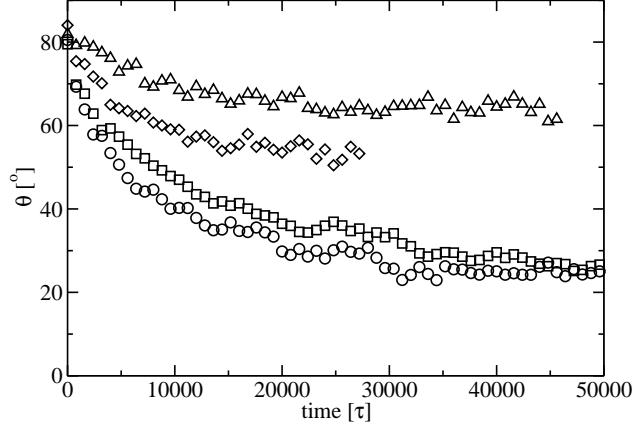


Figure 2: Dynamic contact angle for the binary systems with an equal mixture of  $\varepsilon_w = 0.5\varepsilon$  and  $\varepsilon_w = 1.5\varepsilon$  (triangles) and an equal mixture of  $\varepsilon_w = 1.0\varepsilon$  and  $\varepsilon_w = 2.0\varepsilon$  (squares) compared to the single component droplets with  $\varepsilon_w = 1.5\varepsilon$  (diamonds) and  $\varepsilon_w = 2.0\varepsilon$  (circles).  $N = 10$ ,  $\gamma_L^s = 10.0\tau^{-1}$ .

a monolayer of the  $\varepsilon_w = 3.0\varepsilon$  component still forms at the solid interface since that is the strongly favored interaction. Although earlier simulations showed an accumulation of the more strongly wetting component in the first layer above the substrate,<sup>16</sup> here the first layer consists entirely of the more strongly wetting component. Unlike the  $\varepsilon_w = 1.0\varepsilon/2.0\varepsilon$  case, the spreading rate of the precursor foot is fast enough to allow it to advance well ahead of the bulk of the droplet similar to the leak-out behavior observed experimentally for polymer/solvent mixtures.<sup>3,4</sup> A depletion region forms near the edges of the bulk droplet because the diffusion rate of the wetting component in the bulk is insufficient to replace the material forming the precursor foot. In Section 3.3 we return to this case for varying composition of the two components.

We also consider the case of a droplet containing a mixture of two nonwetting components,  $\varepsilon_w = 0.5\varepsilon$  and  $\varepsilon_w = 1.5\varepsilon$  for  $N = 10$ . As in the previous cases, a monolayer of the more wetting component forms between the droplet and the substrate. In this case, the droplet reaches an equilibrium contact angle of  $\theta_0 \cong 64^\circ$  after  $20\,000\tau$ . The evolution of the contact angle for this nonwetting system is compared to the  $\varepsilon_w = 1.5\varepsilon$  single component system in Figure 2. The single component droplets have equilibrium contact angles of  $\theta_0 \cong 120^\circ$  for  $\varepsilon_w = 0.5\varepsilon$  and  $44^\circ$  for  $\varepsilon_w = 1.5\varepsilon$ . Thus the contact angle of the binary system is more strongly influenced by the material that forms a monolayer on the substrate.

### 3.2 Polymer Chain Length

For droplets composed of two chain lengths of the same type of polymer, the spreading behavior is qualitatively different. The top two droplets in Fig. 3 show profiles for the mixture of chain lengths  $N = 10$  and  $100$  with  $\varepsilon_w = 2.0\varepsilon$  and  $\gamma_L^s = 10.0\tau^{-1}$ . Although  $\varepsilon_w = 2.0\varepsilon$  for both components, the longer chains are in

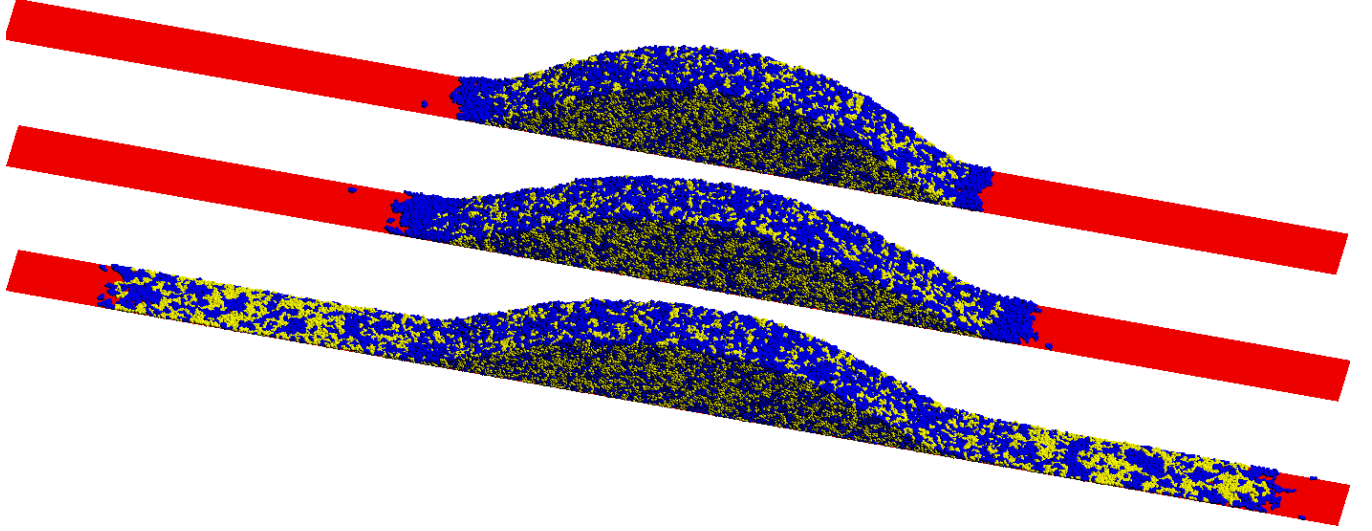


Figure 3: Profiles for binary droplets composed of equal number of monomers of chain length  $N = 10$  (blue) and  $N = 100$  (yellow) polymers with  $\varepsilon_w = 2.0 \varepsilon$  and  $\gamma_L^s = 10.0 \tau^{-1}$  at  $t = 40\,000 \tau$  (top) and  $t = 80\,000 \tau$  (middle). Same as above with  $\varepsilon_w = 3.0 \varepsilon$  and  $\gamma_L^s = 3.0 \tau^{-1}$  taken at  $t = 40\,000 \tau$  (bottom). The substrate (red) has a length of  $800 \sigma$  and a width of  $40 \sigma$  in each profile.

the nonwetting regime ( $\varepsilon_w^c \simeq 2.25 \varepsilon$ )<sup>19</sup> whereas the shorter chains are slightly above the wetting transition ( $\varepsilon_w^c \simeq 1.75 \varepsilon$ ). As a result, a slow precursor foot consisting of approximately 80%  $N = 10$  monomers and 20%  $N = 100$  monomers extends from the bulk region. This is somewhat similar to the “leak-out” behavior observed experimentally in mixtures of polymer and solvent where the precursor foot consists entirely of solvent.<sup>3,4</sup> Unlike Fig. 1, a monolayer of the wetting component does not form on the substrate below the bulk region of the droplet. Instead, the first monolayer at the substrate beneath the droplet consists of an equal fraction of the two components. This can be understood by noting that the longer chains are nonwetting in this case due to their greater surface tension. The chains that are buried beneath the droplet feel no influence of the liquid/vapor interface, so there is no preference as to which chain length is in contact with the substrate. The chains at the upper surface of the droplet, both in the bulk region and the precursor foot, are influenced by the liquid/vapor interface and there one finds an abundance of the shorter chains. The liquid/vapor surface tensions for the  $N = 10$  and  $N = 100$  chains were previously found to be  $0.84$  and  $0.96 \pm 0.02 \varepsilon/\sigma^2$ , respectively.<sup>19</sup> The surface tension for the 10/100 mixture was found to be  $0.90 \pm 0.02 \varepsilon/\sigma^2$  indicating a roughly equal influence by each component on the surface tension of the mixture. Thus, the surface tension calculation is not precise enough to account for the abundance of shorter chains at the liquid/vapor interface.

If  $\varepsilon_w$  is increased so that both chain lengths are in the wetting regime, the behavior is similar to that of a single-component droplet. This is shown in the bottom of Fig. 3 for the mixture of chain lengths  $N = 10$

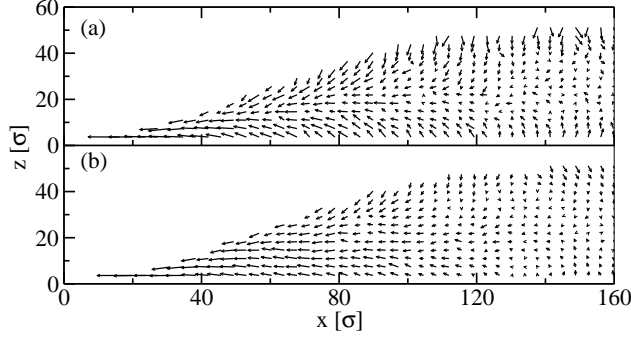


Figure 4: Velocity profiles of half of the droplet showing the  $N = 10$  chain length (a), and the  $N = 100$  chain length (b), for the binary droplet with  $\varepsilon_w = 3.0\varepsilon$  and  $\gamma_L^s = 3.0\tau^{-1}$  at  $t = 20\,000\tau$ .

and 100 where  $\varepsilon_w = 3.0\varepsilon$  and  $\gamma_L^s = 3.0\tau^{-1}$ . Here, both chain lengths are in the wetting regime and the rapidly spreading precursor foot is composed of an equal number of monomers of the two chain lengths. One consequence of this is the  $N = 100$  chains diffuse across the substrate more rapidly when mixed with  $N = 10$  chains than in the pure  $N = 100$  droplet. Although the longer chains have a higher surface tension, the equilibrium state for both components is a  $0^\circ$  contact angle so there is no segregation of the two components in the precursor foot as this droplet spreads. The lack of segregation for a mixture of two chain lengths with the same  $\varepsilon_w$  was previously reported by Voué *et al.* for chain lengths 8 and 16.<sup>16</sup>

The droplet velocity profiles provides another method to analyze the dynamics of the spreading droplet. Figure 4 shows the velocity profiles for the mixture of chain lengths 10 and 100. Although both components show the same spreading pathway, the shorter chain lengths tend to move slightly faster at the liquid/vapor and liquid/solid interfaces.

### 3.3 Varying Composition

The ability to form a film from a non- or weakly wetting polymer by adding a wetting component is of significant practical interest. To analyze the effects of the concentration of the two components on the spreading dynamics, we simulate droplets containing a strongly wetting component ( $\varepsilon_w = 3.0\varepsilon$ ) at different mole fractions,  $x_{wet} = 0.10, 0.25$ , and  $0.50$  with a weakly wetting component ( $\varepsilon_w = 2.0\varepsilon$ ). Since  $N = 10$  for both, the only difference in the two components is the surface interaction. Profiles of the spreading droplets after  $60\,000\tau$  are shown in Figure 5. In each case, a monolayer of the strongly wetting component forms on the surface and spreads outward. The rest of the drop then spreads on this layer. However, for  $x_{wet} = 0.10$ , the surface monolayer never becomes fully homogeneous as a segment of the weakly wetting component remains at the edge of the foot and continues to get pushed outward as the droplet spreads. The size of the depletion region at the droplet edge increases as  $x_{wet}$  decreases since less of the strongly wetting

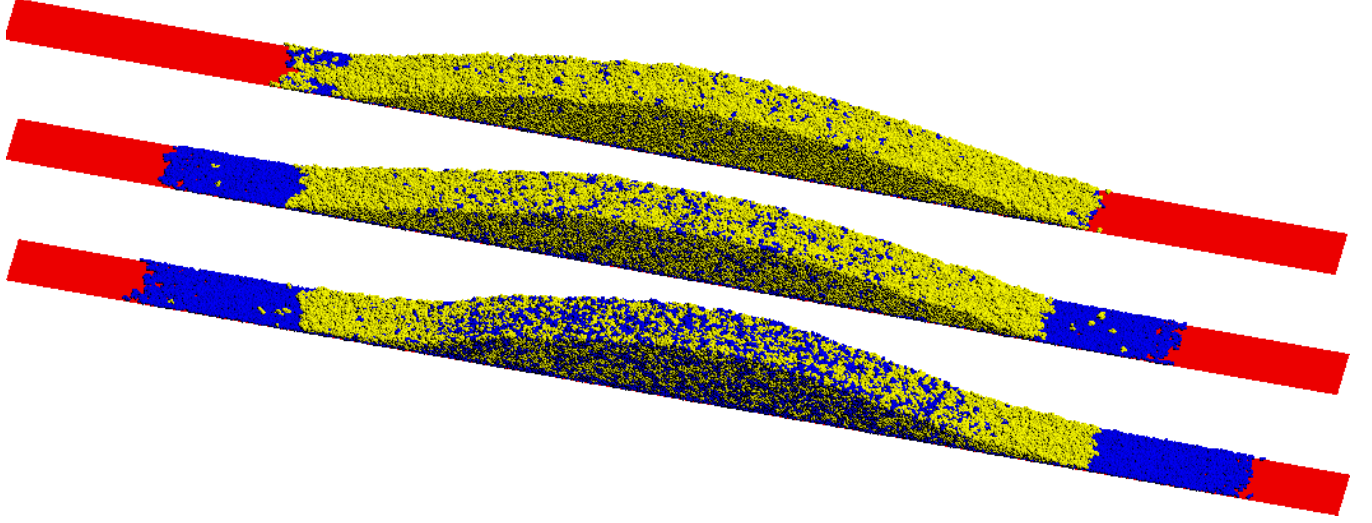


Figure 5: Profiles of three binary droplets of chain length  $N = 10$  with  $\varepsilon_w = 2.0\varepsilon$  (yellow) and  $\varepsilon_w = 3.0\varepsilon$  (blue). The mole fractions of the strongly wetting component are  $x_{wet} = 0.10$  (top),  $0.25$  (middle), and  $0.50$  (bottom).  $t = 60\,000\tau$ ,  $\gamma_L^s = 10.0\tau^{-1}$ . The substrate (red) has a length of  $800\sigma$  and a width of  $40\sigma$  in each profile.

polymer is available to form the precursor foot. The rate of spreading of the precursor foot decreases as  $x_{wet}$  decreases because the supply rate of the strongly wetting material from the bulk to the surface limits the spreading rate of the precursor foot. This is more clearly demonstrated in Fig. 6 where the contact radii of both the foot and bulk regions are shown as a function of time for each of the three compositions and compared to previous results<sup>19</sup> for  $x_{wet} = 0$ . Figure 6a shows that the precursor foot spreading rate decreases as  $x_{wet}$  is reduced. The effective diffusion constant of the precursor foot,  $D_{eff} = \frac{1}{2} \frac{dr_f^2}{dt}$ , decreases from  $4.7$  to  $3.8$ ,  $2.6$  and  $0.6\sigma^2/\tau$  as  $x_{wet}$  decreases from  $0.50$  to  $0.25$ ,  $0.10$  and  $0.0$ , respectively. Figure 6b shows no significant effect of  $x_{wet}$  on the bulk droplet spreading rate for the duration of the simulation for  $x_{wet} = 0.5$  to  $x_{wet} = 0.1$ . However, there is a strong effect on the spreading rate when increasing the concentration from  $x_{wet} = 0.0$  to  $x_{wet} = 0.1$ . In all of these cases, the bulk contact radius spreads as  $t^x$  with  $x \cong 1/5$ ,<sup>19</sup> which is expected from the kinetic model for spreading in the cylindrical geometry used here.

The velocity profiles of the strongly wetting and weakly wetting components at  $t = 70\,000\tau$  are shown in Fig. 7 for  $x_{wet} = 0.25$ . After the foot has extended and a depletion region has formed at the edge of the droplet, Fig. 7a shows that the weakly wetting material moves down from the liquid/vapor surface and up from the solid/liquid surface to allow the monolayer of the strongly wetting material to form. Very little motion is seen in the center of the droplet. In Fig. 7b, the strongly wetting material shows similar behavior at the liquid/vapor surface, but the data is noisier due to the smaller mole fraction of strongly wetting material. This material moves through the depletion region at the edge of the droplet and onto

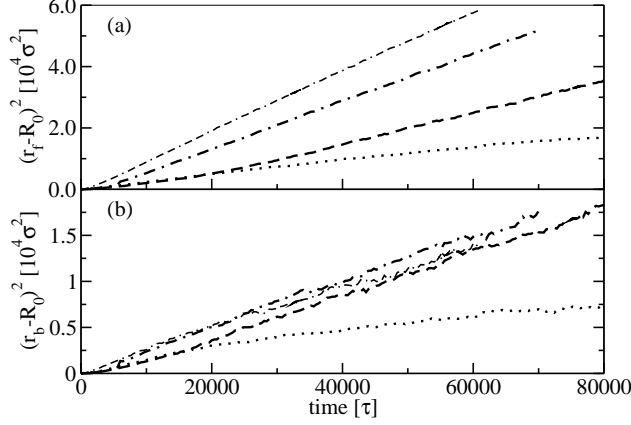


Figure 6: Contact radii of the precursor foot (a) and bulk (b) for the droplets composed of  $x_{wet} = 0$  (dotted curves),  $x_{wet} = 0.10$  (dashed curves),  $0.25$  (dot-dashed curves), and  $0.50$  (dot-dash-dashed curves).  $\varepsilon_w = 2.0\varepsilon$  for the weakly wetting component and  $\varepsilon_w = 3.0\varepsilon$  for the strongly wetting component.  $N = 10$ ,  $\gamma_L^s = 10.0\tau^{-1}$ .

the precursor foot where it rapidly diffuses outward. The same qualitative behavior is observed for different values of  $x_{wet}$ , though the data becomes increasingly noisy as  $x_{wet}$  decreases.

## 4 Conclusions

The spreading dynamics of binary polymer nanodroplets are studied using molecular dynamics simulation. We demonstrate qualitative differences in the spreading behavior of binary droplets due to differences in surface interaction strength, polymer chain length, and composition.

When the two droplet components differ in surface interaction strength, the more strongly wetting component forms a monolayer film on the surface even when both materials are either above or below the wetting transition. For cases that also produce a rapidly spreading precursor foot, a depletion region of the more strongly wetting component forms starting at the edge of the droplet since the interdiffusion rate in the droplet is slower than the rate at which material is withdrawn into the precursor foot.

For differences in the polymer chain length, the monolayer film beneath the droplet is composed of an equal amount of short chain and long chain monomers. This is true even when one component (the shorter chain length) is above the wetting transition and the other is not. In this case, the precursor foot is composed primarily of the wetting component. When both components are above the wetting transition, the surface monolayer and precursor foot are both composed of an equal amount of short and long chain monomers.

The formation of a monolayer of the more strongly wetting component is studied in greater detail by considering different compositions of the mixture of strongly wetting and weakly wetting components. For

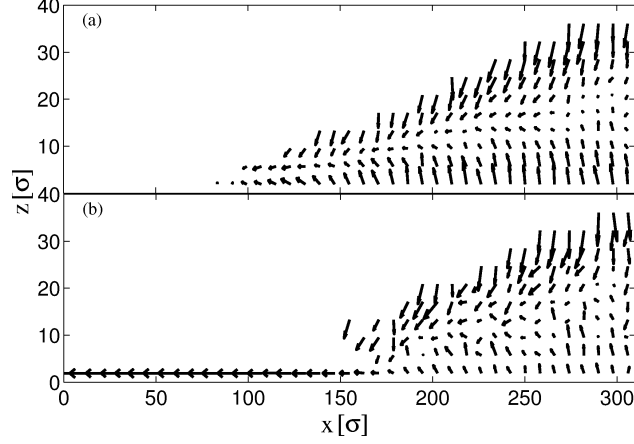


Figure 7: Velocity profiles of half of the droplet showing the weakly wetting component,  $\varepsilon_w = 2.0 \varepsilon$  (a), and the strongly wetting component,  $\varepsilon_w = 3.0 \varepsilon$  (b), for the  $x_{wet} = 0.25$  binary droplet of chain length  $N = 10$  with  $\gamma_L^s = 10.0 \tau^{-1}$  at  $t = 70\,000 \tau$ .

each case, a monolayer of the strongly wetting component forms on the surface and spreads outward. The spreading rate of this precursor foot decreases as the concentration of the strongly wetting component is reduced, but the spreading rate of the bulk droplet shows no significant dependence on the droplet composition until all of the more strongly wetting component is removed. Velocity profiles show that the material for the precursor foot is supplied by the wetting material near the liquid/vapor surface as it diffuses through the depletion region and onto the substrate.

## Acknowledgements

Sandia is a multiprogram laboratory operated by Sandia Corporation, a Lockheed Martin Company, for the United States Department of Energy's National Nuclear Security Administration under Contract No. DE-AC04-94AL85000.

## References

- (1) Keurentjes, J. T. F.; Cohen Stuart, M. A.; Brinkman, D.; Schroën, C. G. P. H.; van't Riet, K. *Colloids and Surfaces* **1990**, *51*, 189.
- (2) Redon, C.; Ausserre, D.; Rondelez, F. *Macromolecules* **1992**, *25*, 5965.
- (3) Fondécave, R.; Brochard-Wyart, F. *Europhys. Lett.* **1997**, *37*, 115.
- (4) Brochard-Wyart, F.; Fondécave, R.; Boudoussier, M. *Int. J. Eng. Sci.* **2000**, *38*, 1033.
- (5) Steiner, U.; Klein, J.; Eiser, E.; Budkowski, A.; Fetters, L. J. *Science* **1992**, *258*, 1126.
- (6) Posazhennikova, A. I.; Indekeu, J. O.; Ross, D.; Bonn, D.; Meunier, J. *J. Stat. Phys.* **2003**, *110*, 611.
- (7) Yeh, M. C.; Chen, L. J. *J. Chem. Phys.* **2003**, *118*, 8331.
- (8) Liu, H.; Bhattacharya, A.; Chakrabarti, A. *J. Chem. Phys.* **1998**, *109*, 8607.
- (9) Toxvaerd, S. *Phys. Rev. Lett.* **1999**, *83*, 5318.
- (10) Ayyagari, C.; Bedrov, D.; Smith, G. D. *Polymer* **2004**, *45*, 4549.
- (11) Puri, S.; Binder, K. *Phys. Rev. A* **1992**, *46*, R4487.
- (12) Kerle, T.; Klein, J.; Binder, K. *Phys. Rev. Lett.* **1996**, *77*, 1318.
- (13) Puri, S.; Binder, K. *Phys. Rev. Lett.* **2001**, *86*, 1797.
- (14) Nieminen, J. A.; Ala-Nissila, T. *Europhys. Lett.* **1994**, *25*, 593.
- (15) Nieminen, J. A.; Ala-Nissila, T. *Phys. Rev. E* **1994**, *49*, 4228.
- (16) Voué, M.; Rovillard, S.; De Coninck, J.; Valignat, M. P.; Cazabat, A. M. *Langmuir* **2000**, *16*, 1428.
- (17) Webb III, E. B.; Hoyt, J. J.; Grest, G. S.; Heine, D. R. *Acta Materialia* (in review).
- (18) Heine, D. R.; Grest, G. S.; Webb III, E. B. *Phys. Rev. E* **2003**, *68*, 061603.
- (19) Heine, D. R.; Grest, G. S.; Webb III, E. B. *Phys. Rev. E* **2004**, *70*, 011606.
- (20) Kremer, K.; Grest, G. S. *J. Chem. Phys.* **1990**, *92*, 5057.
- (21) Grest, G. S.; Kremer, K. *Phys. Rev. A* **1986**, *33*, 3628.
- (22) Braun, O. M.; Peyrard, M. *Phys. Rev. E* **2001**, *63*, 046110.
- (23) Plimpton, S. *J. Comput. Phys.* **1995**, *117*, 1.